

# Action potential restitution and hysteresis in a reaction-diffusion system with pacing rate dependent excitation threshold

J. M. Starobin\*

*University of North Carolina at Greensboro, Greensboro, NC and  
Mediwave Star Technology, Inc., Greensboro, NC*

C. P. Danford, V. Varadarajan, A. J. Starobin, and V. N. Polotski

*Mediwave Star Technology, Inc., Greensboro, NC*

(Dated: February 6, 2020)

## Abstract

We have demonstrated that rate dependent restitution of an excitable medium and action potential duration-refractory period hysteresis can be reproduced in a one-dimensional two-variable Chernyak-Starobin-Cohen reaction-diffusion medium with variable resting potential. We show that restitution and hysteresis depend on the relationship between pacing period and steady state resting potential and also on the rate of resting potential adaptation after an abrupt change in pacing period. It was also observed that for any given value of resting potential, the minimal stable wavefront speed could be approximated by the analytical critical speed of a stable solitary pulse in an infinite cable. This approximation was suitably accurate at a distance from the pacing site regardless of the adaptation constant of resting potential or the dependence of resting potential on pacing interval.

---

\*Electronic address: [jmed@infionline.net](mailto:jmed@infionline.net)

## I. INTRODUCTION

Repetitive pacing of biological reaction diffusion media by over-threshold stimuli gives rise to periodically propagating excitation waves. In cardiac tissue the duration of excitation referred to as action potential duration,  $T_{AP}$ , as well as the speeds of excitation wavefront and waveback, depend on previous stimulation periods and refractory (diastolic) intervals,  $T_{DI}$  [1, 2, 3]. The analysis of such dependences known as restitution curves has been established as an effective method for evaluation of normal functioning of the heart [4, 5, 6, 7, 8, 9].

Pioneering experimental studies [10, 11, 12] established two major pacing sequences such as steady state (dynamic) and S1-S2 pacing protocols, which led to two standard  $T_{AP}$  restitution dependences. It has been shown that the protocol dependent rates of  $T_{AP}$  adaptation were different for stepwise S1-S2 perturbations of cycle length acceleration and deceleration [12, 13]. This phenomenon was later experimentally introduced as action potential duration cycle length hysteresis [14, 15] and has been recently associated with cardiac ischemia and coronary flow reduction [16, 17].

A stepwise change in pacing rate following by sufficiently large number of conditioning S1 stimuli may result in a prolonged adaptation of action potential to its new steady-state level. The process of such adaptation can extend well beyond the  $T_{AP}$  response to the first S2 test stimulus [11, 12] and give rise to the additional constant BCL (basic cycle length) transient restitution component attributed to cardiac memory [2, 18, 19, 20]. Relationship between this phenomenon and stability of pulse propagation as well as with rate dependent  $T_{AP}$ - $T_{DI}$  hysteresis has been recently investigated in experimental [17, 18, 20, 21] and theoretical [22, 23, 24, 25, 26] studies.

It has been found that in the presence of restitution transients cardiac dynamics is more complex than predicted by Nolasco and Dahlen restitution criterion [27]. Specifically, it was demonstrated that dynamic restitution curve slopes  $> 1$  may not automatically indicate loss of excitation wave stability and subsequent appearance of alternans [18, 22, 23, 24, 25, 28]. Computational experiments with Fenton-Karma (FN) reaction-diffusion model readily identified that such effects can be quantified by fitting  $T_{AP}$  and  $T_{DI}$  for specific restitution curves using time dependent gate variables [5, 22, 23].

In this paper, we analyze excitation wave propagation in a one-dimensional cable based on the approach, which follows from direct experimental observations of the dependence

of cardiac muscle resting potential on frequency of external pacing [29, 30, 31]. We use a two-variable exactly solvable Chernyak-Starobin-Cohen (CSC) reaction-diffusion model [32, 33] and modify it accordingly to incorporate pacing rate driven adjustments of resting potential. We use a straightforward gating mechanism, which allows us to add to our model an exponential-like evolution of resting potential,  $V_r$ , following stepwise changes in pacing rate [30]. We demonstrate that adaptation of  $V_r$  significantly affects the stability of pulse propagation and gives rise to rate dependent  $T_{AP}$ - $T_{DI}$  hysteresis. In particular, we find that under given medium parameters, regardless of the slopes of restitution curves, the appearance of alternans away from the stimulation site is determined by proximity of the wavefront speed to the minimal speed of a stationary solitary pulse determined analytically in [32].

## II. METHODS

Basic equations which describe a class of exactly solvable models for excitable media have been defined in [32, 33]. Here we introduce the modification of this analytical model with resting potential  $V_r$  adjusting in response to changes in frequency of external pacing. We will consider the model in dimensionless form:

$$\frac{\partial u}{\partial t} = \frac{\partial^2 u}{\partial x^2} - i(u, v) + P(x, t) \quad (1)$$

$$i(u, v) = \begin{cases} \lambda u & \text{for } u < v \\ (u - 1) & \text{for } u \geq v \end{cases}$$

$$\frac{\partial v}{\partial t} = \epsilon(\zeta u + V_r - v) \quad (2)$$

$$\frac{dV_r}{dt} = -\frac{V_r}{\tau} + B(t) \quad (3)$$

$u(x, t)$  and  $v(x, t)$  are a dimensionless membrane potential and dimensionless, slow recovery current, respectively.  $\lambda$ ,  $\epsilon$ , and  $\zeta$  are the model parameters. The scaling of the system is described in Appendix A.

The pacing function,  $P(x, t)$ , represents a stepwise pacing protocol. It is defined as a product of two functions,  $X(x)$  and  $T(t)$ . Each is constructed using the Heaviside step function,  $\Theta(x)$ , as follows:  $X(x) = A[\Theta(x - \delta_1) - \Theta(x - \delta_2)]$  and  $T(t) = \Theta(t_k) - \Theta(t_k + T_s)$ , where  $A$  and  $\delta_2 - \delta_1$  are the amplitude and width of the pulse, respectively;  $T_s$  is the pulse

duration;  $t_k = t_{N(m-1)} + [k - N(m-1)]T_m$  is the instant of time when the  $k^{\text{th}}$  stimulus is delivered;  $N$  is the number of stimuli at each pacing period,  $T_m, T_s < T_m$ ;  $m$  is the pacing plateau index,  $m = 1, \dots, M$ ;  $M$  is the total number of plateaus in the pacing protocol, and  $k$  is an integer,  $k = 1, \dots, NM$ . The number of stimuli  $N$  is the same for all plateaus.

The right-hand term  $B$  in Eq. 3 is controlled by the stepwise evolution of  $P(x, t)$  using a gating mechanism, which is described in Appendix B. This mechanism employs stepwise changes in  $B$ , which result in smooth exponential evolution of the resting potential from one steady-state value to another. We chose a linear dependence to specify the functional relationship between pacing period,  $T_m$ , and steady state resting potential,  $\bar{V}$  (which is proportional to  $B$ , see Appendix B) at the  $m^{\text{th}}$  pacing plateau,

$$\bar{V} = \beta^\pm T_m + \alpha \quad (4)$$

such that the parameters  $\beta^+$  and  $\beta^-$  represented rates of changes of  $\bar{V}$  with increasing and decreasing pacing period,  $T_m$ , respectively, and  $\alpha$  is a constant.

### III. NUMERICAL SIMULATIONS

The system of Eqs. 1-3 was solved numerically on a short cable of 250 grid points with spatial and temporal grid intervals of  $\Delta x = 0.13$  and  $\Delta t = 7.2 \times 10^{-4}$ , respectively. The length of the cable was approximately equal to the width of the pulse to reflect the relative dimensions of the heart and a propagating cardiac pulse at moderate heart rates. Periodic wavetrains were produced by stimulating the cable with a square wave at the left end using the function  $P(x, t) = X(x)T(t)$ , defined above, where  $A = 10$ ,  $\delta_1 = 2\Delta x$ ,  $\delta_2 = 15\Delta x$ , and  $T_s = 10^3\Delta t$ . The model parameters  $\lambda$ ,  $\epsilon$ , and  $\zeta$  were equal to 0.4, 0.1, and 1.2, respectively, for all simulations. Numerical solutions were computed using a second-order explicit-difference scheme [9]. A typical solution is depicted in Fig. 1, showing the nonstationary propagation of a single pulse at three instants of time.

In order to quantify the dynamics of the system (Eqs. 1-3 and B1-B3), we computed the action potential duration,  $T_{AP}$ , the diastolic interval,  $T_{DI}$ , and the wavefront velocity,  $c$ . The action potential duration was defined as the interval of time when  $u > v$  at a specified node,  $x_0$ . Accordingly, the refractory period,  $T_{DI}$ , was defined as the interval of time when  $u < v$ . The speed of the wavefront,  $c$ , was calculated based on the time it took for a point

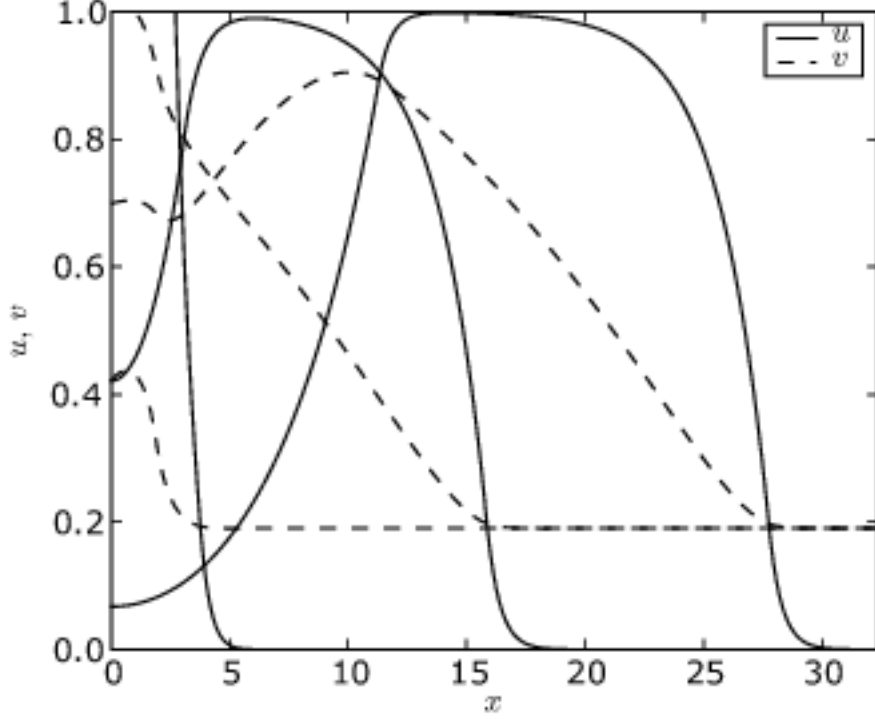


FIG. 1: Spatio-temporal dynamics of  $u, v$  variables. Three snapshots of  $u$  and  $v$  are shown for a resting potential  $V_r = 0.19$ . The first snapshot occurs at the instant of the pacing stimulus and shows the formation of the wavefront. The next two snapshots are taken after periods of 7.2 (20% of the pacing period) and 14.4 and show pulses with accelerating wavefronts and wavebacks.

of constant phase on the wavefront ( $u = 0.5$ ) to travel a span of 10 grid points centered around  $x_0$ . In order to analyze a developed pulse (except Sec. III D), we measured intervals and speeds at  $x_0 = 20$  where the speed of the wavefront had reached a constant steady-state value while the speed of the waveback was still slightly changing.

### A. Restitution for constant resting potential

The system of equations 1-3 was initially studied with Eq. 3 replaced by its degenerate form  $\frac{\partial V_r}{\partial t} = 0$ , which is equivalent to  $\tau = \infty$  and  $B(0) = 0$ . The cable was stimulated periodically with pacing periods ranging from 32 to 70 with increments of 1.5. At a given  $V_r$ , the pacing interval  $T_m$  was kept constant for forty consecutive periods comprising the conditioning S1 plateau. The values of  $T_{AP}$  and  $T_{DI}$  at the end of each conditioning plateau

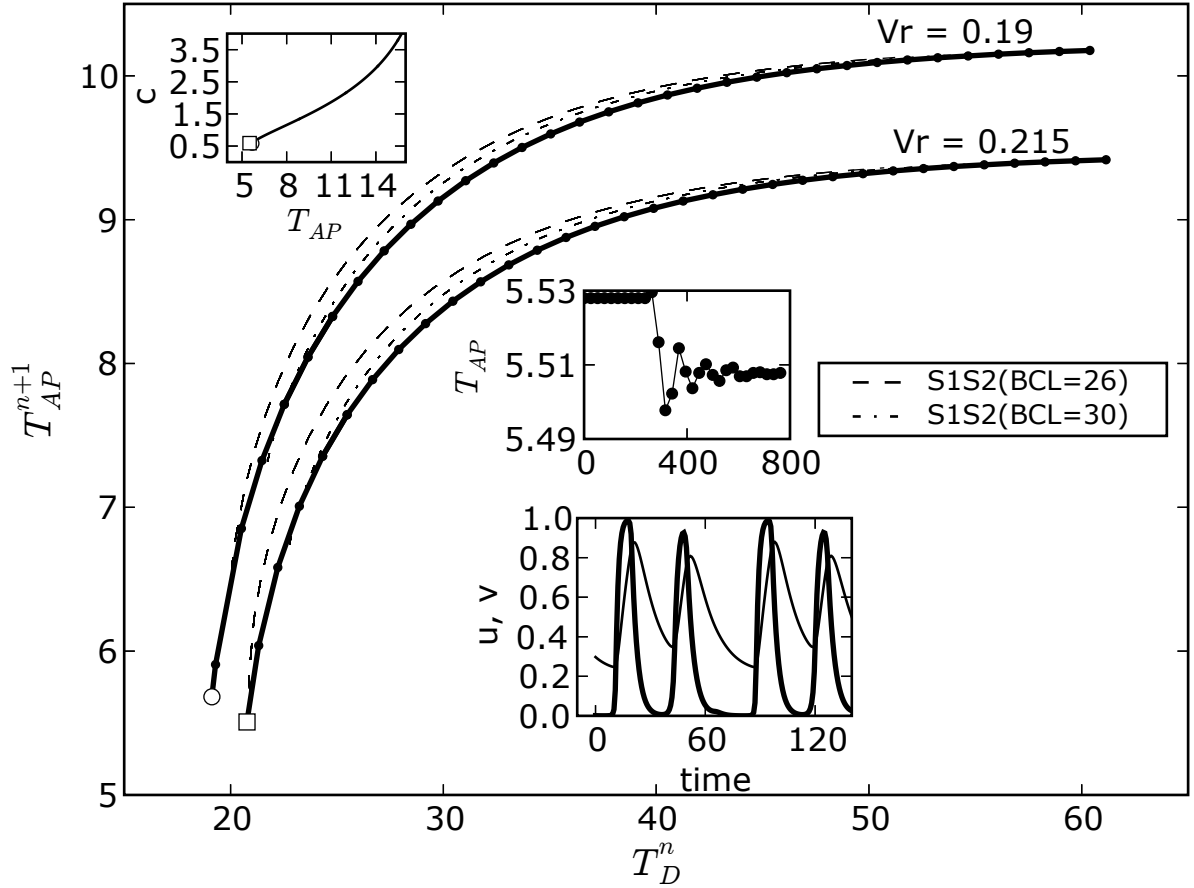


FIG. 2: Steady-state and S1-S2 restitution curves are shown with solid and dashed lines, respectively. Critical  $T_{AP}$  and  $T_{DI}$  values are marked with open markers. The minimal values of  $T_m$  and  $T_{AP}$  which corresponded to these critical points were  $T_m^{crit} = 24.8$ ,  $T_{AP}^{crit} = 5.7$  and  $T_m^{crit} = 26.3$ ,  $T_{AP}^{crit} = 5.5$  for  $V_r = 0.19$  and  $V_r = 0.215$ , respectively.

composed the steady state restitution curve. The pulse,  $T_{AP}^{n+1}$ , resulting from the premature stimulus, S2, following the conditioning sequence and the last diastolic interval,  $T_{DI}^n$ , from the conditioning S1 plateau composed the S1-S2 restitution curve.

Steady state and S1-S2 restitution curves computed for a pair of constant resting potentials are shown in Fig. 2. We observed that the maximal difference between steady state and S1-S2 restitution curves comprised less than 15% of the corresponding steady state value of  $T_{AP}$ , which implied that transient responses to any premature stimulus were on average limited to just a single non-stationary pulse.

The open markers at the ends of both steady state restitution curves shown in Fig. 2 indicate the critical points below which no stable propagation and no 1 : 1 responses were observed. We found that even an insignificant decrease of the pacing interval towards the critical value of  $T_m^{crit} = 26.3$  at  $V_r = 0.215$  resulted in oscillations of action potential duration shown in the mid level insert panel. Further reduction of the pacing interval from  $T_m^{crit} = 26.3$  to  $T_m = 25.9$  induced even more complex 3 : 2  $T_{AP}$  response pattern depicted in the lower level insert panel.

The upper level insert panel shows the dispersion curve computed analytically for a steady state solitary pulse [32]. This insert demonstrates that the difference between numerical (open marker) and analytical (the end of the solid line) critical stable propagation speeds is relatively small and amounts only to 10% of the wavefront speed determined from our numerical model at  $V_r = 0.215$ . On the contrary, the maximum slope of the dynamic restitution curve for the same  $V_r$  was 30% greater than the Nolasco-Dahlen critical stability slope of one [27].

## B. Restitution and hysteresis for rate-dependent $V_r$

Unlike the previous section, the evolution of  $V_r$  according to Eq. 3 resulted in a set of prolonged transients initiated by abrupt changes in stimulation rate. These  $T_{AP}$  transients, which constituted the constant BCL restitution (negative slope, Fig. 3A), had a duration of 5-50 stimulation periods depending on the adaptation constant,  $\tau$  (Fig. 3D). The phase of constant BCL adaptation followed the immediate S1-S2 responses, which were on the contrary positive and aligned with the steady state restitution curves for each steady state  $V_r$  (gray lines, Fig. 3A).

Different steady state values of  $V_r$  during a there and back stepwise stimulation protocol gave rise to  $T_{AP}$ - $T_{DI}$  hysteresis. The cable was stimulated periodically for fifty consecutive periods at a series of conditioning plateaus. The series consisted of five plateaus with decreasing  $T_m$  followed by the same number of plateaus with increasing  $T_m$ . The resting potential evolved according to Eq. 3, and its steady state value at each plateau was related to the pacing period by Eq. 4.

Using this protocol we demonstrated that higher values of  $T_{AP}$ - $T_{DI}$  hysteresis corresponded to greater differences between  $\beta^+$  and  $\beta^-$  during the decremental and incremental

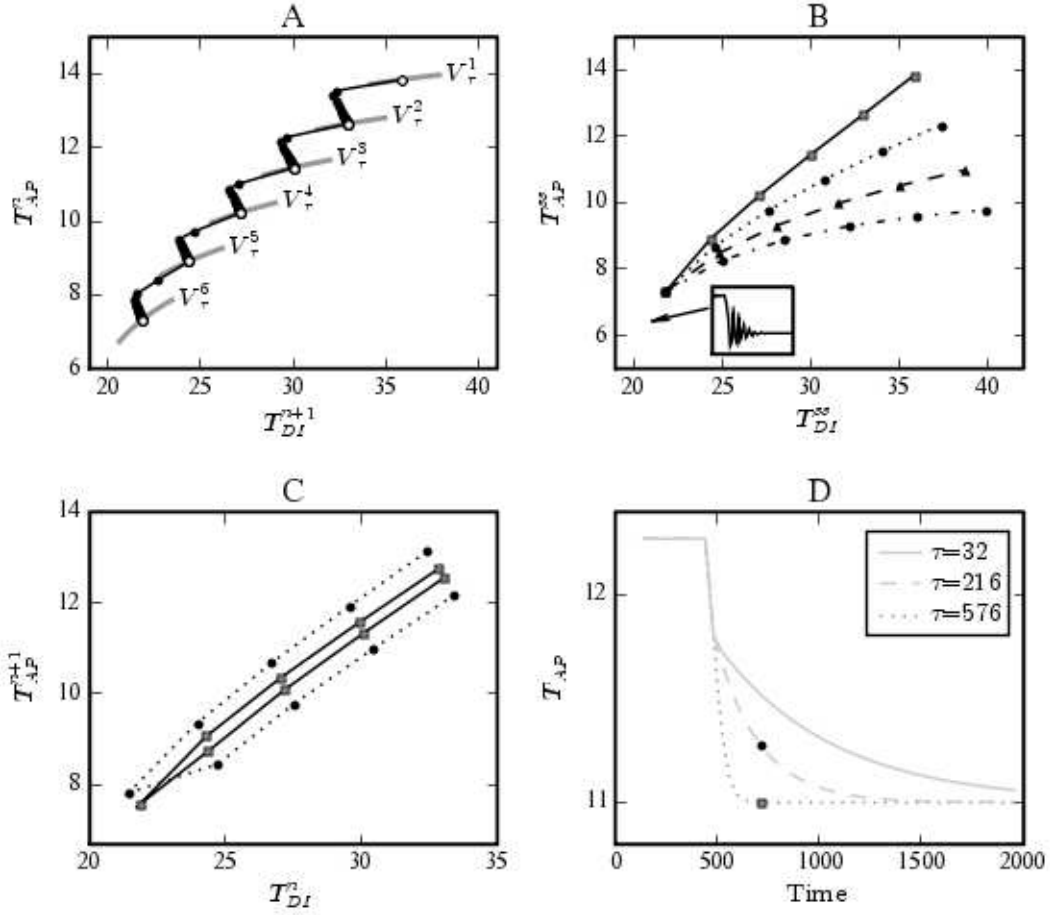


FIG. 3: Restitution relations and  $T_{AP}-T_{DI}$  hysteresis for a stepwise stimulation protocol with rate dependent  $V_r$ . (A) Sequential  $T_{AP}$  and  $T_{DI}$  are shown as black circles. Open circles mark steady-state  $T_{AP}$  and  $T_{DI}$  intervals. Portions of constant resting potential,  $V_r^i$ , and steady state restitution curves are shown in gray. (B)  $T_{AP}-T_{DI}$  hysteresis produced by increasing differences between  $\beta^+$  and  $\beta^-$ .  $\beta^+ = 6 \times 10^{-3}$  for the top curve (solid line, squares),  $\beta^- = 4 \times 10^{-3}$  (dotted line, solid circles),  $\beta^- = 2 \times 10^{-3}$  (dashed line, triangles), and  $\beta^- = 0.1 \times 10^{-3}$  for the lowest curve (dash-dotted line, circles). Portions of the constant  $V_r$  steady state restitution curves are shown in gray for comparison. The inset depicts the onset of alternans when the stimulation interval was decreased further than the end of the curves ( $T_m = 27.9$ ). (C)  $T_{AP}-T_{DI}$  hysteresis for different values of the adaptation constant,  $\tau$  ( $\tau = 216$ , dotted line;  $\tau = 32$ , solid line), when  $\beta^+ = \beta^-$ . (D) Adaptation of action potential duration after an abrupt decrease in stimulation interval for three different rate constants ( $\beta^+ = 6 \times 10^{-3}$ ). The measured transient intervals in Panel C are highlighted with the same markers.

stages of the pacing protocol (Fig. 3B). We also found that  $T_{AP}$ - $T_{DI}$  hysteresis was dependent on the adaptation constant,  $\tau$ , if  $T_{AP}$  and  $T_{DI}$  were measured before their steady-state values were reached. For instance, for a time lag of seven stimulation intervals and  $\beta^+ = \beta^- = 6 \times 10^{-3}$  (Fig. 3D), the magnitude of  $T_{AP}$ - $T_{DI}$  hysteresis increased as the adaptation constant increased from  $\tau = 32$  to  $\tau = 216$  (Fig. 3C).

### C. Transitions to $T_{AP}$ alternans, and comparison with stability of a solitary pulse

When the pulse duration and speed are less than certain critical values, steady-state solitary pulse and wavetrain propagation in an infinite cable do not exist [32, 33]. Such critical values for a solitary pulse occur at the end of the solitary pulse’s dispersion curve, as computed analytically in [32]. Similar critical values for our short cable were described in Sec. III A for a medium with constant resting potential, and we expected oscillations of  $T_{AP}$  and wavefront speed to arise when steady state pulse speeds decrease below their critical value.

The inset panels A and B in Fig. 4 show the responses of  $T_{AP}$  to abrupt changes in stimulation period,  $T_m$ , and resulting exponential evolution (Eq. 3) of resting potential. Both pulse duration and resting potential were slightly perturbed around their critical values as indicated by the arrow labelled “A,B” (Fig. 4). The shortening of  $T_m$  triggered  $V_r$  to increase above the critical level. These changes caused  $T_{AP}$  to approach gradually a critical value below which a bifurcation (alternans) occurred (insert B, open markers at the end of the arrow).  $T_{AP}$  and wavefront speed alternated between two stable values. Alternans occurred sooner when the adaptation rate was higher due to smaller constant (insert A). On the contrary, when the perturbation of  $T_{AP}$  did not reach the critical value (inserts C and D), for example when the initial stimulation period was greater ( $T_m = 57.6$ ) but  $\beta^+$  was the same, similar bifurcations did not occur. Instead, we observed typical exponential adaptation from one steady-state to another.

As in the previous section our numerical simulations reveal that away from stimulation site stability of propagation is predominantly determined by the critical solitary pulse speed. Indeed, as  $\beta^+$  increased, the maximal slopes of steady state restitution curves significantly increased from 1.4 to 5.7 while the critical wavefront speeds indicated at the curves in Fig. 5 were practically the same. On the contrary, closer to the stimulation site at  $x_0 = 4$  the

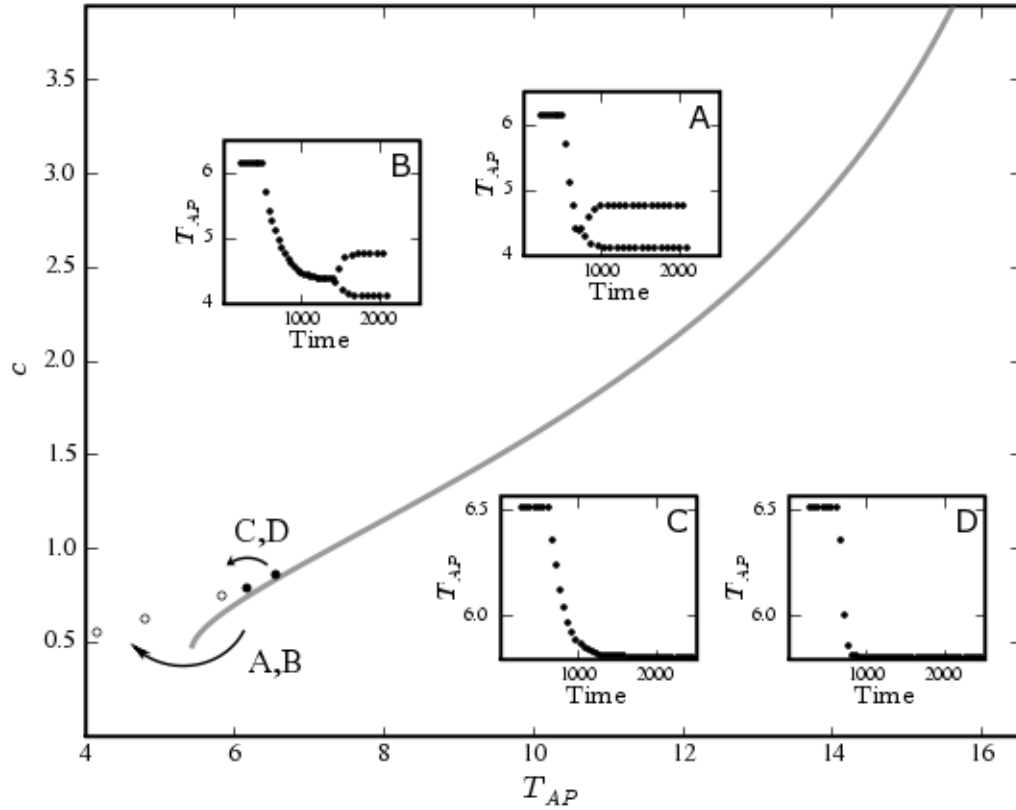


FIG. 4: Initiation of instability of  $T_{AP}$  in a finite cable away from the stimulation site at  $x_0 = 20$ . Inserts show  $T_{AP}$  response to a perturbation in stimulation rate, for initial  $T_m = 46.8$  and  $\beta^+ = 2 \times 10^{-3}$ . (A) and (B) depict alternans of  $T_{AP}$  when the adaptation constant is small ( $\tau = 32$  in A) and large ( $\tau = 216$  in B). (C) and (D) depicts stable transitions of  $T_{AP}$  for the same adaptation constants ( $\tau = 216$  in C;  $\tau = 32$  in D) when the stimulation interval is greater. Gray line in main panel depicts dispersion curve of a steady-state solitary pulse [32]. The markers at the left end of the dispersion curve show the starting speed and  $T_{AP}$  (solid circles) and the ending speeds and  $T_{AP}$  (open circles) for both inserts.

critical wavefront speed was twice as great as the critical speed of the steady state solitary pulse. The next section provides more details about these dynamics.

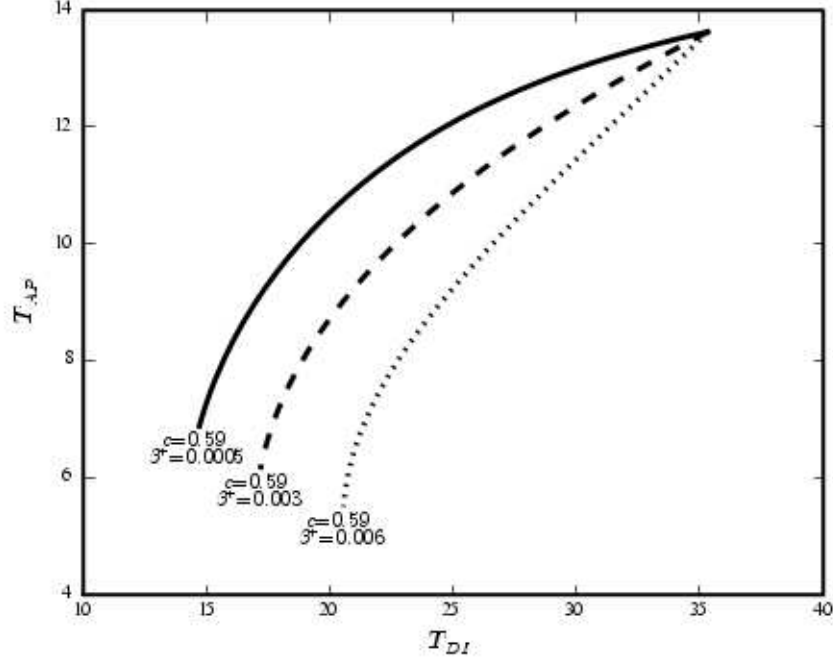


FIG. 5: Steady state restitution for three different rate dependences of the steady state resting potential.  $\tau = 216$  for all curves.

#### D. Influence of propagation in the cable of finite length

Comparisons of  $T_{AP}$ - $T_{DI}$  hysteresis were made between measurements close to ( $x_0 = 4$ ) and at a distance from the stimulation site ( $x_0 = 20$ ) when the wavefront speed has decreased to a steady state value. Figure 6 shows that both the magnitude of hysteresis and  $T_{AP}$  increased by almost a factor of two further from the stimulation site.

We found that the onset of alternans was different near the site of stimulation and far from it. Figure 7A demonstrates that an abrupt change in  $T_m$  initiates prolonged (20 pacing periods) exponential adaptation of  $T_{AP}$  at a distance from the stimulation site. During this adaptation, the wavefront speed decreased until the critical value,  $c = 0.59$  (Fig. 5), at which time a bifurcation occurred, and  $T_{AP}$  started to alternate. On the contrary, close to the stimulation site (Fig. 7B),  $T_{AP}$  alternans started almost immediately after three stimuli following the change in pacing period.

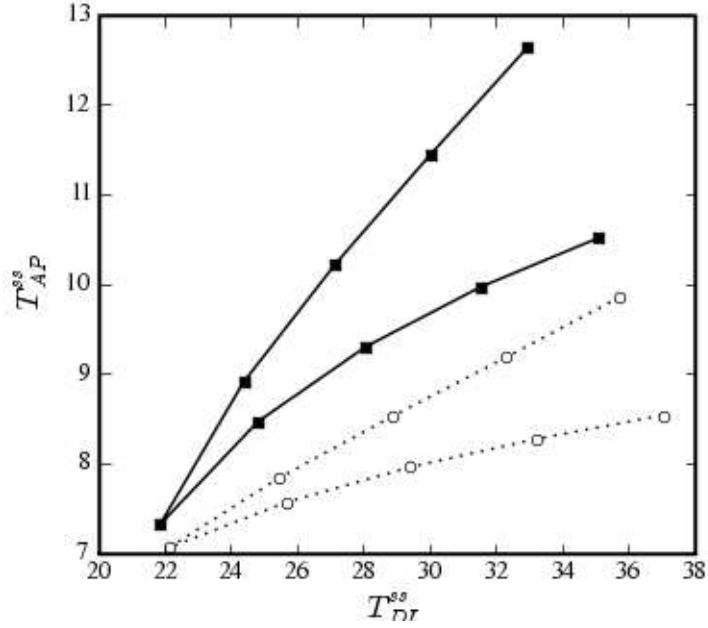


FIG. 6: Steady-state  $T_{AP}$ - $T_{DI}$  hysteresis at  $x_0 = 4$  (dashed line, open circles) and  $x_0 = 20$  (solid line, squares). For both curves,  $\beta^+ = 6 \times 10^{-3}$ , and  $\beta^- = 2 \times 10^{-3}$ .

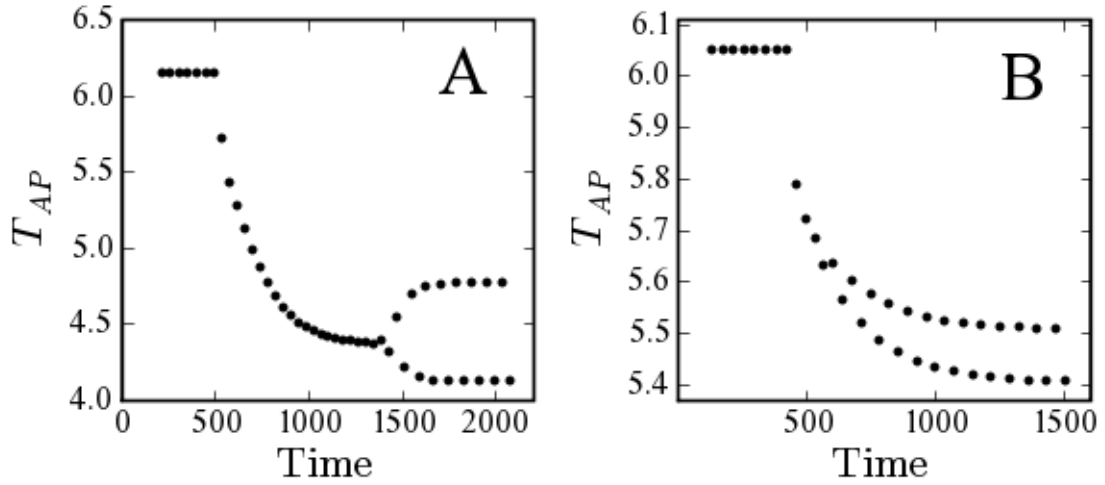


FIG. 7: The onset of alternans at different distances from the stimulation site. Oscillations were induced by perturbing  $T_{AP}$  and  $V_r$  around their critical values, with  $T_m = 65$ ,  $\beta^+ = 1.4 \times 10^{-3}$ . Panels A and B show the onset of alternans at  $x_0 = 20$  and  $x_0 = 4$ , respectively.

## IV. CONCLUSIONS

We have demonstrated that rate dependent restitution and  $T_{AP}$ - $T_{DI}$  interval hysteresis can be reproduced in a one-dimensional two-variable CSC reaction-diffusion medium where resting potential adjusts to changes in pacing rate. We show that the rate dependence of restitution and hysteresis are influenced by two major factors. The first one is the rate,  $\beta^\pm$ , of change of steady-state resting potential with increasing and decreasing pacing period. The second is the adaptation constant,  $\tau$ , of resting potential adaptation after an abrupt change in pacing interval. We show that steady-state and S1-S2 restitution curves coincide if the resting potential is constant, which corroborates earlier findings for other reaction diffusion models [3, 24, 26]. On the contrary, the steady-state and S1-S2 restitution curves diverge if the magnitude of resting potential varies with changes in pacing rate, leading to prolonged  $T_{AP}$  transients following an abrupt change in pacing interval.

We found that larger values of  $T_{AP}$ - $T_{DI}$  interval hysteresis were associated with greater differences between  $\beta^+$  and  $\beta^-$ . Even if there was no difference between these values, hysteresis resulted from increasing adaptation constants,  $\tau$ , if  $T_{AP}$  and  $T_{DI}$  were measured before their steady-state values were reached.

Our numerical simulations showed that stimulating the cable with very short pacing intervals led to  $T_{AP}$  alternans. We found that the onset of alternans, which occurred after an abrupt change in pacing rate, was more delayed for larger values of  $\tau$ . It was also observed that for any given value of resting potential regardless of  $\beta^\pm$ , the minimal stable wavefront speed could be approximated by the analytical critical speed of a stable solitary pulse in the infinite cable [32, 33]. This approximation was suitably accurate at a distance from the stimulation site regardless of values of  $\beta^\pm$  and magnitudes of the slopes of restitution curves.

### Acknowledgments

This study was funded by Mediwave Star Technology, Inc. and was partially supported by the University of North Carolina at Greensboro. The authors are grateful to Lanty L. Smith and Thomas R. Sloan for their support and critical reviews.

## APPENDIX A:

The scale of  $u$  is the maximum steady-state action potential amplitude  $U_0$ , the scale of  $v$  is given by  $\sigma_f U_0$ , and the time scale is  $C_m/\sigma_f$ , where  $\sigma_f$  corresponds to the maximum sodium conductance and  $C_m$  is the membrane capacitance. The characteristic length scale is given by  $\sqrt{D/\sigma_f}$ , where  $D$  is the diffusion length. The small parameter  $\epsilon \ll 1$ , is equal to  $C_m/(\tau_s \sigma_f)$  and  $\zeta = \sigma_s/\sigma_f$  where  $\sigma_s$  corresponds to the maximum potassium conductance.

## APPENDIX B:

The term  $B(t)$  in Eq. 3 is governed by a gating function,  $g(t)$ :

$$\frac{dg}{dt} = \begin{cases} 1 & \text{if } P_s = 0 \\ -D(g - T_s) & \text{if } P_s = A. \end{cases} \quad (\text{B1})$$

where  $D \gg 1/T_s$  such that  $g$  decays rapidly within the interval  $T_s$ , and  $P_s$  is the pacing function at the site of pacing.

We define a variable  $T_g$  whose value is equal to the local maximum of  $g(t)$  in the interval equal to an estimate of the current stimulation period  $T_m$ . A variable  $T_a$  measures this estimate adaptively. The dynamics of  $T_a$  is governed by the following:

$$\frac{dT_a}{dt} = \begin{cases} -D_1(T_a - T_g) & \text{if } P_s = 0 \\ 0 & \text{if } P_s = A. \end{cases} \quad (\text{B2})$$

$D_1$  is chosen such that  $T_a$  decreases at a rate much slower than  $g(t)$  within the stimulation period,  $D \gg D_1 \gg T_m^{-1}$ .

This results in the following delay-differential equation for  $T_g$ :

$$\frac{dT_g}{dt} = \begin{cases} -Dg(t - T_a) & \text{if } g(t) < \max_{\{t-T_g(t) < r < t\}} g(r) = g(t - T_a) \\ 0 & \text{if } g(t) < \max_{\{t-T_g(t) < r < t\}} g(r) < g(t - T_a) \\ 1 & \text{if } g(t) = \max_{\{t-T_g(t) < r < t\}} g(r) > g(t - T_a). \end{cases} \quad (\text{B3})$$

Changes of  $B(t)$  are then defined synchronously with changes in  $T_g(t)$  and  $T_g(t - T_g)$  ac-

ording to the following equation:

$$B(t) = \begin{cases} B(t - T_g) + \Delta B_m^+ & \text{if } T_g(t - T_g) > T_g(t) \\ B(t - T_g) - \Delta B_m^- & \text{if } T_g(t) > T_g(t - T_g) \\ B(t - T_g) & \text{if } T_g(t) = T_g(t - T_g). \end{cases} \quad (\text{B4})$$

$\Delta B_m^+$  and  $\Delta B_m^-$  are increment values corresponding to decreasing or increasing  $T_m$ , respectively. Stepwise increments,  $\Delta B_m^+$ , (or decrements,  $\Delta B_m^-$ ) result in a smooth exponential increase (or decrease) of  $V_r$ , where  $\Delta B_m^\pm = \frac{\beta^\pm \Delta T_m}{\tau}$  for each plateau. The resulting steady-state resting potential is proportional to  $B(t)$  with a multiplicative factor  $\tau$ . Figure 8 illustrates the adaptation of  $B(P(x, t))$  and  $V_r$  in response to changes in pacing period,  $T_m$ .

According to Eq. B4,  $g(t)$  increases linearly when  $P_s$  is zero (between adjacent stimuli) and decays rapidly otherwise. Therefore at the points of local maxima its value is equal to  $T_m$ . This rapid decay in  $T_g(t)$  when  $T_m$  decreases occurs at the same rate as  $g(t)$ . According to Eq. B2, any change in  $T_g(t)$  results in a slow convergence of  $T_a$  to the new stimulation period  $T_m$ . An appropriate choice of the rate constant  $D_1$  as indicated above ensures that this convergence occurs within the stimulation interval. When there is an increase in  $T_m$ ,  $T_g$  increases linearly to the new local maxima of  $g(t)$  in the interval  $T_a$ . Finally Eq. B4 incorporates a stepwise decrease or increase in  $B$  depending on the difference between  $T_g(t)$  and its shifted value  $T_g(t - T_g)$  (demonstrated in the 3<sup>rd</sup> and 4<sup>th</sup> panels of Fig. 8).

- 
- [1] D. Chialvo, D. Michaels, and J. Jalife, *Circulation Research* **66**, 525 (1990).
  - [2] R. Gilmour, N. Otani, and M. Watanabe, *American Journal of Physiology - Heart and Circulatory Physiology* **272**, H1826 (1997).
  - [3] J. Cain, E. Tolkacheva, D. Schaeffer, and D. Gauthier, *Physical Review E* **70**, 061906 (2004).
  - [4] A. Karma, *Chaos* **4**, 461 (1994).
  - [5] F. Fenton and A. Karma, *Chaos* **8**, 20 (1998).
  - [6] A. Garfinkel, Y. Kim, O. Voroshilovsky, Z. Qu, J. Kil, M. Lee, H. Karagueuzian, J. Weiss, and P. Chen, *Proceedings of the National Academy of Sciences* **97**, 6061 (2000).
  - [7] Z. Qu, A. Garfinkel, P. Chen, and J. Weiss, *Circulation* **102**, 1664 (2000).
  - [8] I. Schwartz, I. Triandaf, J. Starobin, and Y. Chernyak, *Physical Review E* **71**, 7208 (2000).

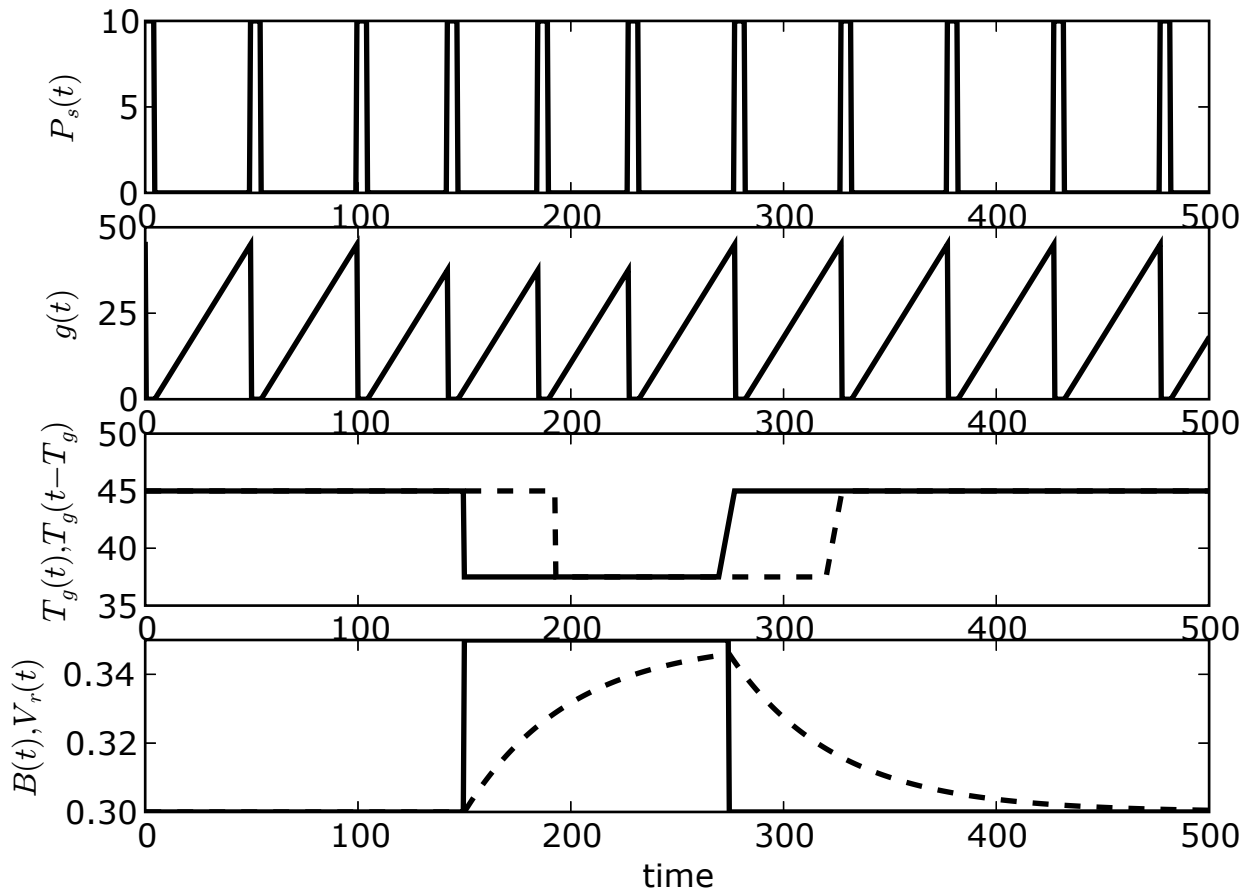


FIG. 8: Changes in  $B(t)$  and  $V_r(t)$  in response to pacing period,  $T_m$ . Adaptation of the gating function  $g(t)$  and corresponding evolution in  $T_g(t)$  (solid line, panel 3) and time-shifted  $T_g(t - T_g)$  (dashed line, panel 3) with pacing  $P(x, t)$  is depicted.

- [9] Y. Chernyak and J. Starobin, *Critical Reviews in Biomedical Engineering* **27**, 359 (1999).
- [10] M. Boyett and B. Jewell, *Journal of Physiology* **285**, 359 (1978).
- [11] V. Elharrar and B. S. B., *American Journal of Physiology - Heart and Circulatory Physiology* **244**, H782 (1983).
- [12] M. Franz, C. Swerdlow, L. Liem, and J. Schaefer, *Journal of Clinical Investigation* **82**, 972 (1988).
- [13] L. Arnold, J. Page, D. Attwell, M. Cannell, and D. Eisner, *Cardiovascular Research* **16**, 547 (1982).
- [14] J. S. Sarma, S. Venkataraman, D. Samant, and U. Gadgil, *Pacing and Clinical Electrophysi-*

- ology **10**, 485 (1987).
- [15] A. Krahn, G. Klein, and R. Yee, *Circulation* **96**, 1551 (1997).
  - [16] M. Lauer, C. Pothier, Y. Chernyak, R. Brunken, M. Lieber, C. Apperson-Hansen, and J. Starobin, *Journal of Electrocardiology* **39**, 315 (2006).
  - [17] J. Starobin, W. Cascio, A. Goldfarb, V. Varadarajan, A. Starobin, C. Danford, and T. Johnson, *Journal of Electrocardiology* **40**, S91 (2007).
  - [18] M. Hall, S. Bahar, and D. Gauthier, *Physical Review Letters* **82**, 2995 (1999).
  - [19] N. Otani and R. Gilmour, *Journal of Theoretical Biology* **187**, 409 (1997).
  - [20] S. Kalb, H. Dobrovolny, E. Tolkacheva, S. Idriss, and W. Krassowska, *Journal of Cardiovascular Electrophysiology* **15**, 698 (2004).
  - [21] M. Watanabe and M. Koller, *American Journal of Physiology - Heart and Circulatory Physiology* **282**, H1534 (2002).
  - [22] F. Fenton, S. Evans, and H. Hastings, *Physical Review Letters* **83**, 3964 (1999).
  - [23] E. Cherry and F. Fenton, *American Journal of Physiology - Heart and Circulatory Physiology* **286**, H2332 (2004).
  - [24] E. Tolkacheva, D. Schaeffer, D. Gauthier, and C. Mitchell, *Chaos* **12**, 1034 (2002).
  - [25] E. Tolkacheva, D. Schaeffer, D. Gauthier, and W. Krassowska, *Physical Review E* **67**, 031904 (2003).
  - [26] S. Kalb, E. Tolkacheva, D. Schaeffer, D. Gauthier, and W. Krassowska, *Chaos* **15**, 023701 (2005).
  - [27] J. Nolasco and R. Dahlen, *Journal of Applied Physiology* **25**, 191 (1968).
  - [28] I. Banville and R. Gray, *Journal of Cardiovascular Electrophysiology* **13**, 1141 (2002).
  - [29] D. Attwell, I. Cohen, and D. Eisner, *Journal of Physiology* **313**, 439 (1981).
  - [30] J. Davidenko, R. Levi, G. Maid, M. Elizari, and M. Rosenbaum, *American Journal of Physiology - Heart and Circulatory Physiology* **259**, H290 (1990).
  - [31] U. Ravens and E. Wettwer, *Basic Research in Cardiology* **93**, 60 (1998).
  - [32] Y. Chernyak, J. Starobin, and R. Cohen, *Physical Review Letters* **80**, 5675 (1998).
  - [33] Y. Chernyak, J. Starobin, and R. Cohen, *Physical Review E* **58**, R4108 (1998).